Human Molecular Genetics, 2020, Vol. 29, No. 12 2051–2064

doi: 10.1093/hmg/ddaa084
Advance Access Publication Date: 18 May 2020
General Article

GENERAL ARTICLE

Loss of *Snord116* alters cortical neuronal activity in mice: a preclinical investigation of Prader–Willi syndrome

Marta Pace[1,†,§], Ilaria Colombi[1,2,§], Matteo Falappa[1,2,§], Andrea Freschi[1], Mojtaba Bandarabadi[3,‡], Andrea Armirotti[4], Blanco María Encarnación[4], Antoine R. Adamantidis[3,5], Roberto Amici[6], Matteo Cerri[6], Michela Chiappalone[7,*,¶,††] and Valter Tucci[1,*,††]

[1]Genetics and Epigenetics of Behaviour (GEB), Istituto Italiano di Tecnologia (IIT), Genova 16163, Italy, [2]Dipartimento di Neuroscienze, Riabilitazione, Oftalmologia, Genetica e Scienze Materno-Infantili (DINOGMI), Università degli Studi di Genova, Genova 16132, Italy, [3]Centre for Experimental Neurology, Department of Neurology, Inselspital University Hospital, University of Bern, Bern 3010, Switzerland, [4]Analytical Chemistry Facility, Istituto Italiano di Tecnologia (IIT), Genova 16163, Italy, [5]Department of Clinical Research, Inselspital University Hospital, University of Bern, Bern 3010, Switzerland, [6]Department of Biomedical and NeuroMotor Sciences, Alma Mater Studiorum—University of Bologna, Bologna 40126, Italy and [7]Rehab Technologies, Istituto Italiano di Tecnologia (IIT), Genova 16163, Italy

*To whom correspondence should be addressed at: Neurobehavioural Genetics Group, NBT—IIT Via Morego 30, Genova 16163, Italy. Tel: +39 010 2896 747; Email: valter.tucci@iit.it; Rehab Technologies Lab, IIT Via Morego 30, Genova 16163, Italy. Tel: +39-010 71781743; Email: michela.chiappalone@iit.it

Abstract

Prader–Willi syndrome (PWS) is a neurodevelopmental disorder that is characterized by metabolic alteration and sleep abnormalities mostly related to rapid eye movement (REM) sleep disturbances. The disease is caused by genomic imprinting defects that are inherited through the paternal line. Among the genes located in the PWS region on chromosome 15 (15q11-q13), small nucleolar RNA 116 (*Snord116*) has been previously associated with intrusions of REM sleep into wakefulness in humans and mice. Here, we further explore sleep regulation of PWS by reporting a study with PWScr$^{m+/p-}$ mouse line, which carries a paternal deletion of *Snord116*. We focused our study on both macrostructural electrophysiological components of sleep, distributed among REMs and nonrapid eye movements. Of note, here, we study a novel electroencephalography (EEG) graphoelements of sleep for mouse studies, the well-known spindles. EEG biomarkers are often linked to the functional properties of cortical neurons and can be instrumental in translational studies. Thus, to better understand specific properties, we isolated and characterized the intrinsic activity of cortical neurons using *in vitro* microelectrode array. Our results confirm that the loss of *Snord116* gene in mice influences specific properties of REM sleep, such as theta rhythms and, for the first time, the organization of REM episodes throughout sleep–wake cycles. Moreover, the analysis of sleep spindles present novel specific phenotype in PWS mice, indicating that a new catalog of sleep biomarkers can be informative in preclinical studies of PWS.

†Marta Pace, http://orcid.org/0000-0003-1637-4544
‡Mojtaba Bandarabadi, http://orcid.org/0000-0002-4608-1374
¶Michela Chiappalone, http://orcid.org/0000-0003-1427-5147
§Marta Pace, Ilaria Colombi and Matteo Falappa have contributed equally to this work.
††Michela Chiappalone and Valter Tucci jointly supervised this work.
Received: March 4, 2020. **Revised:** April 26, 2020. **Accepted:** April 27, 2020

Introduction

Sleep disturbances are frequently reported in subjects with Prader–Willi syndrome (PWS, OMIM 176270), representing a burden that impacts the quality of life for patients and their families. Indeed, up to 76% of PWS patients exhibit abnormal sleep (1,2). PWS is a neurodevelopmental disorder characterized by hypotonia and failure to thrive in infancy. From ∼2 years of age, the phenotype shifts to hyperphagia, which leads to obesity (3,4). Other phenotypic hallmarks of PWS include mild to moderate cognitive deficits, behavioral problems including obsessive–compulsive disorder, and sleep disturbances. Among the sleep disturbances, excessive daytime sleepiness (EDS) have been mainly reported in PWS subjects (5,6), together with rapid eye movement (REM) sleep dysregulation (7–9). However, in addition to REM dysregulation, a number of important features of mammalian sleep can contribute to produce an irregular sleep–wake cycle (10). Some studies have also reported narcoleptic-like symptoms such as sleep attacks, cataplexy and a transient loss of muscle tone (7,11).

PWS is caused by the lack of expression of paternally expressed genes in the chromosomal region 15q11-q13. The small nucleolar RNA (snoRNA) clusters in this region have a pivotal role in the etiology of the disease. Individuals lacking the SNORD116 snoRNA cluster (imprinted in PWS) gene suffer the same failure to thrive, hypotonia and hyperphagia that are observed in subjects with larger deletions and maternal uniparental disomy (12,13). Additionally, it has been shown that mice with a paternal deletion of the *Snord116* gene ($PWScr^{m+/p-}$) recapitulate the major human endophenotypes, including sleep alteration coupled with dysregulation of diurnal clock genes (14,15).

We have previously described sleep alterations in $PWScr^{m+/p-}$ mice, mostly related to REM sleep (14). Here, we explored specific features of sleep architecture concerning the processes that regulate REM sleep in $PWScr^{m+/p-}$ mice. In addition, we investigated a typical graphoelement of sleep such as sleep spindles, hallmarks of nonrapid eye movement (NREM) sleep. Spindle activity is attributed to interactions among thalamic reticular, thalamocortical (TC) and cortical pyramidal networks (16). Therefore, dysregulation of spindle properties is a sensitive indicator of TC and neuromodulator dysfunction in many diseases, including neurodevelopmental disorders (17). Previous studies have reported a complete absence or dysregulation of sleep spindles in PWS subjects (18,19); however, this component has never been investigated in preclinical models, mainly because of difficulties in studying microstructural electroencephalography (EEG) elements in rodents.

Children with PWS have been shown to have abnormal functional connectivity among brain regions (20), a phenomenon that can derive from cortical and/or subcortical structures. These alterations may impact on the genesis and distribution of spindles during sleep. Therefore, we sought to investigate the regulation of sleep by analyzing electrophysiological elements dependent on the TC projections and intrinsic cortical processes. To investigate the properties of intrinsic cortical connectivity, with no interference from external stimuli and from the TC projections (21), we studied *in vitro* cultures of dissociated cortical neurons using microelectrode array (MEA) recordings.

Our results confirm the function of the *Snord116* gene in sleep regulation and extend our understanding of sleep in PWS. Moreover, they address, for the first time, the role of *Snord116* in regulating the sleep macrostructure and that of the TC/cortical processes in controlling sleep architecture.

Results

Paternal *Snord116* deletion impacts the sleep macrostructure and the graphoelement typical of sleep in mice

To assess whether *Snord116* might contribute to sleep disturbances associated with PWS, we recorded the sleep–wake cycle over the 24-h circadian period (12 h:12 h light/dark cycle) of $PWScr^{m+/p-}$ and $PWScr^{m+/p+}$ mice (Fig. 1A). Both genotypes exhibited the typical circadian change in the sleep–wake distribution, with reduced sleep (NREM and REM sleep) during the dark hours compared with the light hours (Supplementary Material, Fig. S2A). Total sleep and wake duration showed no obvious differences between the two cohorts of mice (Supplementary Material, Fig. S2A). In contrast, the total amount of REM sleep was increased in mice lacking a paternal *Snord116 gene* during the dark period ($PWScr^{m+/p+}$ 2.425 ± 0.5083 versus $PWScr^{m+/p-}$ 3.865 ± 0.4334, $t(18) = 2.15$, $P = 0.04$; Fig. 1B). Next, we assessed the EEG power spectra, and delta (4–4.5 Hz) power density during NREM sleep was found to be significantly reduced in the $PWScr^{m+/p-}$ mice compared with the control mice (two-way ANOVA: $F(39, 351) = 44.13$ $P < 0.0001$; 'frequency Hz'; Supplementary Material, Fig. S2B).

Since the EEG analysis highlighted an alteration of REM sleep, which reflects a change in the distribution of REM periods with no effects on total sleep or wakefulness, we further explored the duration of REM sleep episodes in detail. Our results show, for the first time, the presence of a bimodal distribution of REM sleep interval (RSI) in mice. RSI was bimodally distributed in both genotypes of mice over the 24-h circadian period, with the two clusters separated at 55 s, which accounts for the minimum frequency (Fig. 1C). Based on these parameters, the two detected subpopulations of RSI were used to distinguish single REM sleep episodes (long RSI > 60 s) and sequential REM sleep episodes (short RSI ≤ 60 s). Although a bimodal distribution was observed in both genotypes of mice, the frequency of short RSIs was significantly higher in the $PWScr^{m+/p-}$ mice than in the $PWScr^{m+/p+}$ mice ($PWScr^{m+/p+}$ 3.40 ± 0.99 versus $PWScr^{m+/p-}$ 7.6 ± 1.6, $t(18) = 2.21$, $P = 0.03$; Fig. 1C), suggesting a high REM sleep propensity in the mutant mice. Conversely, the numbers of long RSIs were unchanged between the two genotypes (Fig. 1C). In addition, the REM–NREM cycle was analyzed as an identifier of sleep propensity (22). Our data showed that the cycle length was ∼2–5 min in both genotypes of mice, as already described (23). However, in the $PWScr^{m+/p-}$ mice, a large increase in REM–NREM cycles was observed over the 24 h of the sleep–wake cycle ($PWScr^{m+/p+}$ 9.00 ± 2.06 versus $PWScr^{m+/p-}$ 15.15 ± 1.51, $t(18) = 2.40$, $P = 0.02$; Fig. 1C).

Paternal deletion of *Snord116* alters sleep spindles in PWS mice

Sleep spindle properties were explored in relation to the circadian and homeostatic components of sleep (Fig. 1D). Sleep spindles are the well-characterized sources of EEG power in the 9–16 Hz range during NREM sleep (see Fig. 1E). We calculated these spindle properties for each genotype at different time-points and found that the density of spindles was unchanged between the two genotypes in all investigated conditions (Fig. 1E). However, we observed that spindle duration ($t(1988) = 3.04$, $P = 0.002$; Fig. 1E), central frequency ($t(1988) = 2.70$, $P = 0.006$; Fig. 1E) and the number of spindle cycles ($t(1988) = 3.47$, $P = 0.005$; Fig. 1E) were significantly increased in the $PWScr^{m+/p-}$ mutants compared with the control mice. Conversely, spindle amplitude was

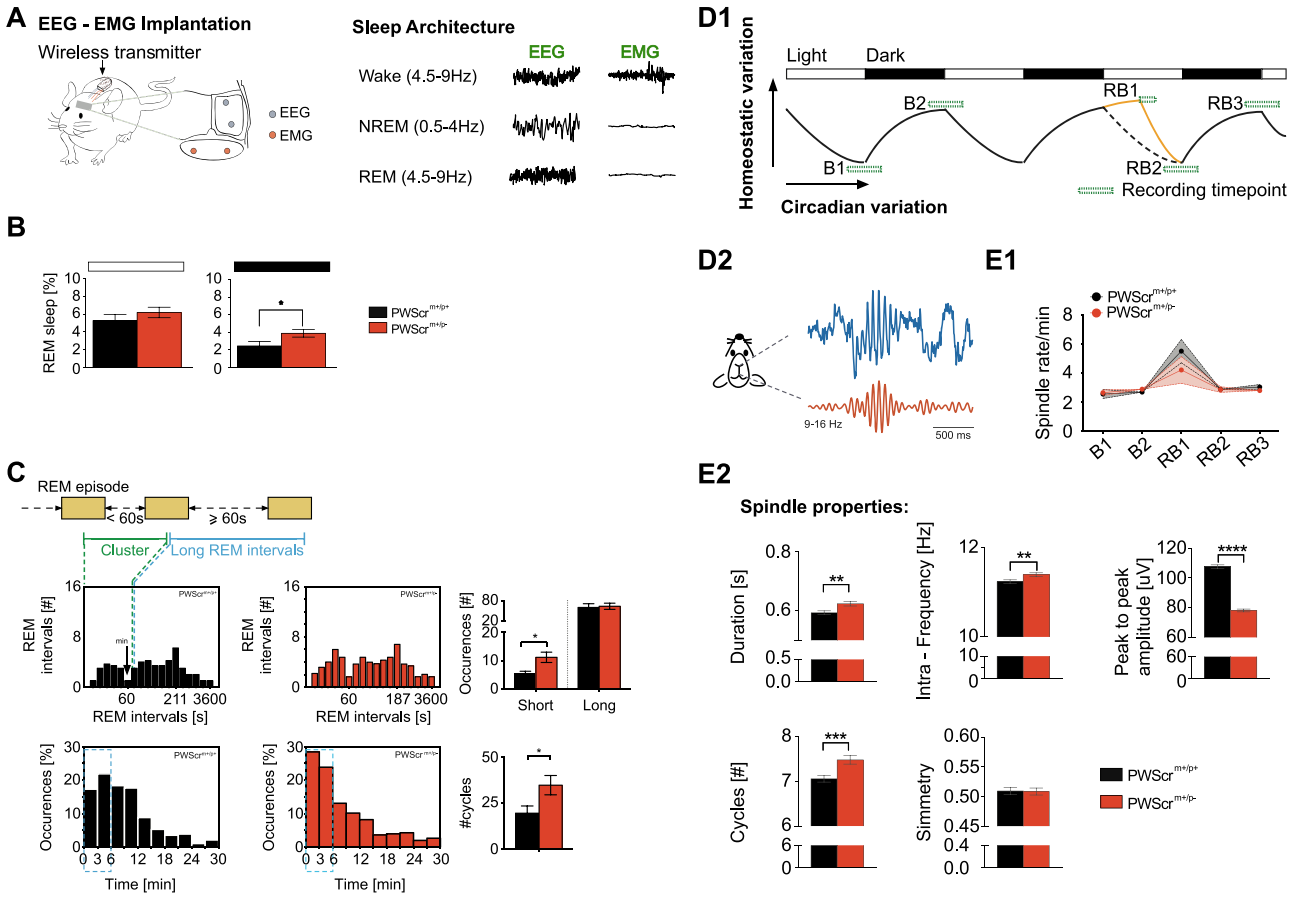

Figure 1. Paternal *Snord116* deletion impacts REM sleep and NREM sleep spindles. **(A)** Schematic representation of EEG/EMG implantation to assess the sleep architecture characterized by wake, NREM and REM sleep. **(B)** The percentage of time spent in REM sleep during the 12 h light and dark periods for PWScr$^{m+/p-}$ mice (red) versus controls (black). Values are the 12 h means ± SEM. **(C)** On the top, schematic representation of the criteria used to distinguish the short- and long-RSI. In the middle, the average frequency distribution of the duration of the interval from the end of one REM sleep episode to the beginning of the next REM sleep episode (RSI) recorded over the 24 h of the sleep–wake cycles in PWScrm$^{+/p+}$ ($n = 10$ in black) and PWScrm$^{+/p-}$ mice ($n = 10$ in red). The frequency class, which was taken as the boundary separating short- and long-interval populations (minimum), was at 55 s. On the right, the average value of the occurrence of the short- and long-RSI for each genotype. On the bottom, histograms of the length of the sleep–wake cycle over the 24 h in PWScrm$^{+/p+}$ ($n = 10$ in black) and PWScrm$^{+/p-}$ mice ($n = 10$ in red). Sleep cycles—length was plotted for 3-h bins. Only data up to 30 min is shown, for more details regarding the criteria used, see Materials and Methods section. On the right, the average value of the number of the cycle length ~2–5 min in both genotypes of mice. **(D1)** Schematic representation of experimental design to record sleep spindles properties. Sleep spindles were recorded at different time-point according to the circadian and homeostatic sleep control. At the baseline, sleep spindles were recorded at two time-points (B1 and B2) for 2 h between the shift from the light and dark period and vice versa, indicated by a green square. Next, sleep spindles were recorded over the first hour of the rebound period (RB1) following 6 h of total sleep deprivation and in other two time-points over the 18 h of recovery period (RB2 and RB3). **(D2)** Schematic representation of the spindles signal. **(E1)** The number of the spindles estimated over the 24 h of the sleep–wake cycles in both genotypes, PWScrm$^{+/p+}$ ($n = 10$ in black) and PWScrm$^{+/p-}$ mice ($n = 10$ in red). **(E2)** Sleep spindles properties: duration between 0.4 and 2 s, central frequency, peak-to-peak amplitude, number of cycles between 5 and 30 and symmetry. Values are expressed as mean ± SEM. *$P < 0.05$; **$P < 0.01$; ***$P < 0.001$.

significantly lower in the PWScr$^{m+/p-}$ mutants compared with the PWScr$^{m+/p+}$ mice ($t(1988) = 18.59$, $P < 0.0001$; Fig. 1E).

PWS mutants show increased spontaneous physical activity over the circadian cycle

Physical activity was assessed in awake mice without any motor constraints. During the 24 h of the circadian period, both genotypes showed an increase in physical activity during the night and a decrease in motility during the day. Interestingly, mutant mice displayed an increase in spontaneous physical activity during the subjective night (light phase, resting phase for mice) compared with control mice (PWScr$^{m+/p+}$ 2.48 ± 0.44 versus PWScr$^{m+/p-}$ 3.96 ± 0.33, $t(18) = 2.6$, $P = 0.01$; Fig. 2A). Moreover, physical activity was also increased in the mutant mice during the first hours of the dark period compared with the motor activity of control mice (two-way ANOVA: $F(11,99) = 9.318$, $P < 0.0001$, 'time of day', and $F(1,9) = 5.23$, $P = 0.04$, 'groups'; Fig. 2A).

Paternal *Snord116* deletion leads to dysregulation of norepinephrine

Neuromodulators are fundamental players in the regulation of sleep–wake cycles. Here, we report an assessment of the levels of glycine, glutamate, norepinephrine, histamine and gamma-aminobutyric acid (GABA) in the cerebrospinal fluid (CSF) of both genotypes. Notably, among all the investigated neuropeptides, it was found that the levels of norepinephrine, a neurotransmitter that is involved in arousal and is also important for the regulation of REM sleep (24,25), was significantly increased in the PWScr$^{m+/p-}$ mice relative to the control (PWScr$^{m+/p+}$ 0.53 ± 0.07 versus PWScr$^{m+/p-}$ 0.08 ± 0.01, $t(8) = 6.22$, $P = 0.0003$; Fig. 2B).

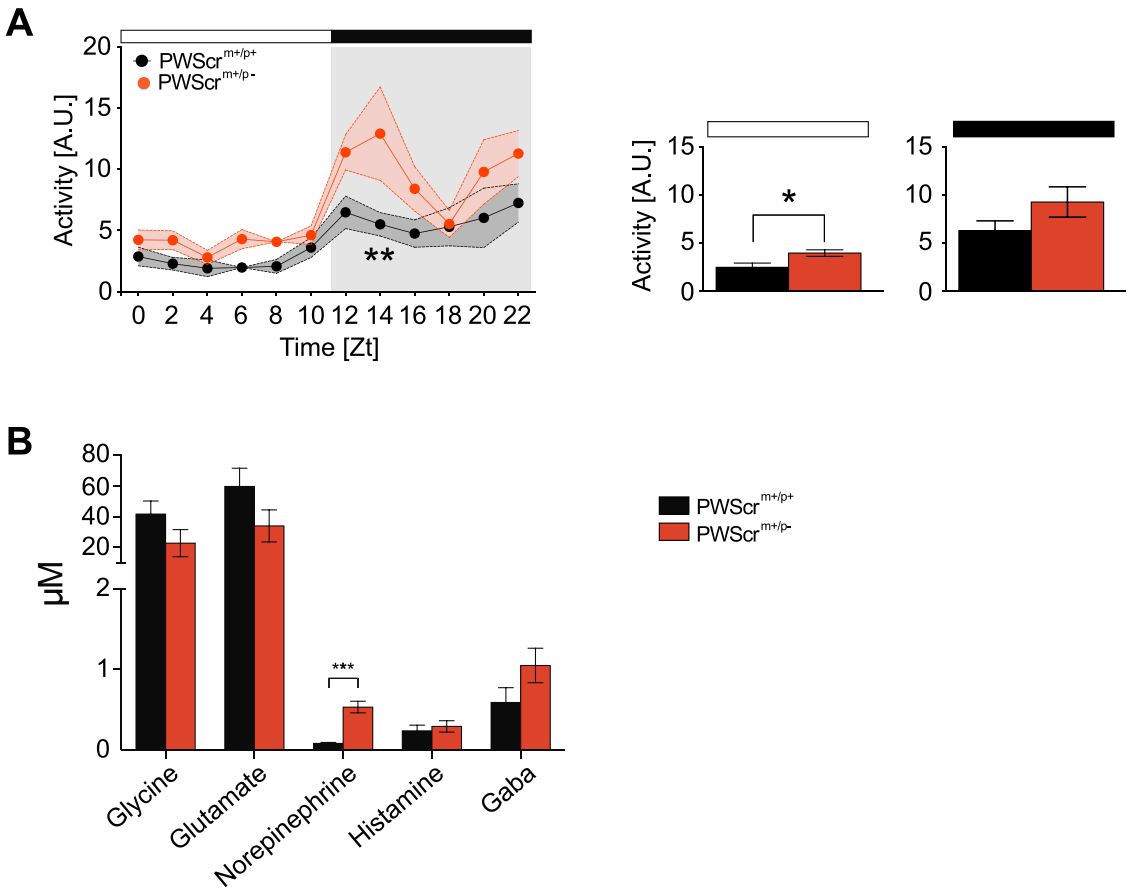

Figure 2. Paternal *Snord116* deletion increases physical activity and norepinephrine levels. (**A**) On the left, telemetry measurements of daily activity in home cages monitored 24 h/day in PWScrm$^{+/p+}$ ($n=10$ in black) and PWScrm$^{+/p-}$ mice ($n=10$ in red). On the right, the spontaneous physical activity averaged during the 12 h light and dark period. Values are the 12 h means ± SEM. (**B**) Levels of neurotransmitters (glycine, glutamate, norepinephrine, histamine and GABA) assessed in the CSF of PWScrm$^{+/p+}$ ($n=10$ in black) and PWScrm$^{+/p-}$ mice ($n=10$ in red). Mice were sacrificed at the beginning of the dark period. Values are expressed as mean ± SEM. $^{*}P<0.05$; $^{**}P<0.01$; $^{***}P<0.001$.

REM-like *in vitro* phenotypes emerge from paternal *Snord116* deletion neurons

To assess whether *Snord116* impacts the communication of cortical networks of neurons isolated from the TC connections, we studied electrophysiological and transcriptional changes in dissociated embryonic cortical neurons obtained from PWScr$^{m+/p-}$ and PWScr$^{m+/p+}$ mice. We administered carbachol (CCh) to the cultures to suppress the delta wave activity and emphasize activity in the theta frequency range. We recorded 2 h of baseline (BL) neuronal activity (i.e. basal phase) in the culture medium, followed by 2 h of CCh administration for both genotypes (PWScr$^{m+/p-}$ and PWScr$^{m+/p+}$ cultures). We compared the electrophysiological activity on two different time scales: local field potential (LFP) and multiunit activity (MUA).

First, we analyzed the low-frequency component of the signal (i.e., LFP) to investigate whether PWScr$^{m+/p-}$ cultures showed an alteration in the theta oscillations during CCh administration. Our results, in agreement with our previous studies, demonstrated dysregulation of the electrophysiological activity in the theta frequency band of PWScr$^{m+/p-}$ mice during REM sleep (14) over the 24-h circadian period (as the BL condition). In the BL condition, cortical networks from both genotypes revealed spontaneous synchronized bursting resembling the slow-wave activity typical of NREM sleep. Indeed, the analysis of the LFP performed in PWScr$^{m+/p-}$ and PWScr$^{m+/p+}$ cultures during spontaneous phase did not indicate differences between the genotypes (Supplementary Material, Fig. S3).

We then stimulated cortical cultures with CCh as previously described (26) (Fig. 3B) and we normalized power with respect to the basal condition. Following CCh administration, the power of the delta waves decreased by 80% in both sets of cultures (Fig. 3C). We found a significant difference between the two sets of cultures (i.e. PWScr$^{m+/p-}$ and PWScr$^{m+/p+}$) only in the theta waves after 1 h of CCh application (time-point = 30′: $q=3.222$; $P=0.029$; time-point = 60′: $q=3.828$; $P=0.011$; time-point = 90′: $q=3.94$; $P=0.009$; time-point = 120′: $q=3.693$; $P=0.013$) (Fig. 3C1). Specifically, the theta power of the control cultures decreased by 60%. In contrast, the theta power of the PWS cultures decreased by 30%. These results are consistent with the results of the *in vivo* experiment that revealed abnormalities in REM sleep characterized by theta waves. Beta waves did not show significant differences between the two genotypes. Detailed statistical information about the multiple comparisons is available in Supplementary Material, Table S5.

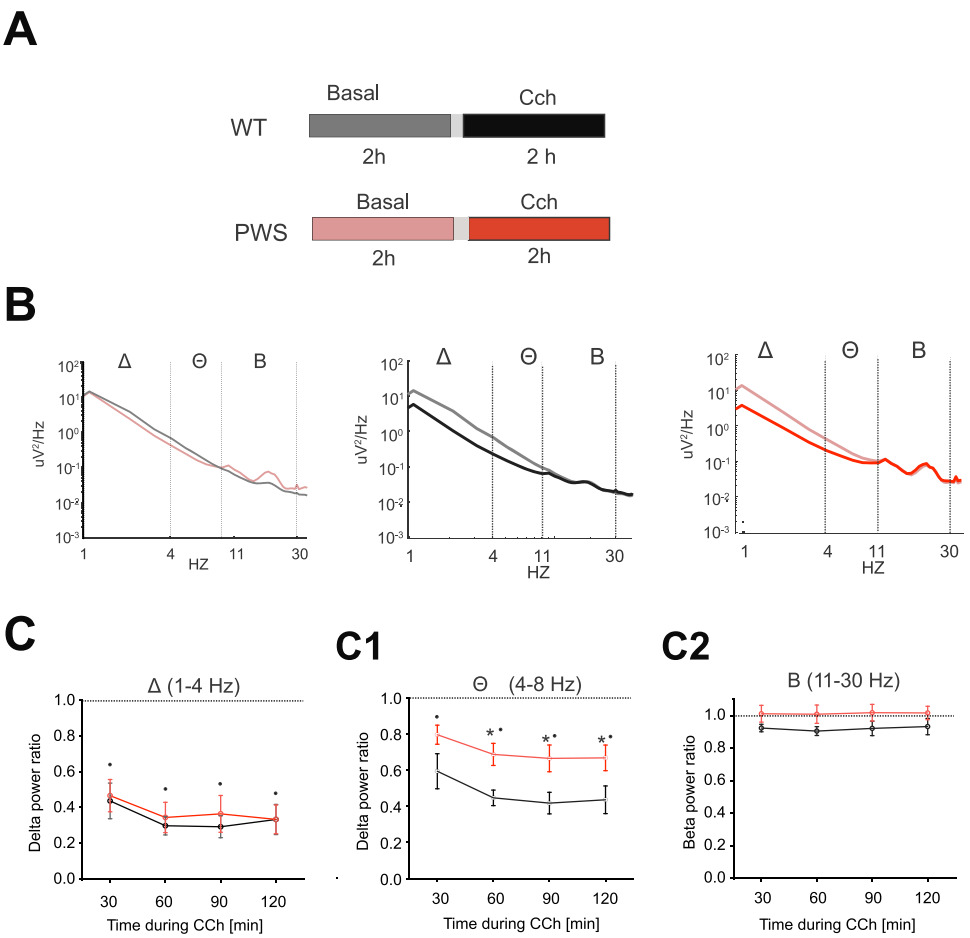

Figure 3. LFP analysis of PWScr$^{m+/p-}$ and PWScr$^{m+/p+}$ cultures. **(A)** The experimental protocol adopted for the experiments. We recorded 2 h of spontaneous phase followed by 2 h of CCh administration. **(B)** (Left) Power spectral density of basal segments for PWScr$^{m+/p-}$ and PWScr$^{m+/p+}$ cultures. We computed the power for each set of bands delta (1–4 Hz), theta (5–9 Hz) and beta (9–13 Hz). We did not find any differences during the basal phase. (Center) Power spectral density of PWScr$^{m+/p+}$ cultures under baseline conditions (gray line) and during CCh application (black line). CCh caused suppression of all the low waves considered. Power spectral density of PWScr$^{m+/p-}$ cultures under baseline conditions (light red line) and during CCh application (red line). **(C)** Delta power following CCh administration. We normalized the power in each band with respect to the basal value (indicated by the dashed line). After dividing the entire recording into 30-min intervals, we did not find a significant difference between PWScr$^{m+/p-}$ and PWScr$^{m+/p+}$ cultures: CCh administration caused a significant decrease in the delta power for both genotype. **(C1)** Theta power following CCh administration. We normalized the power in each band with respect to the basal value (indicated by the dashed line). After dividing the entire recording into 30-min intervals, we found a significant difference between PWScr$^{m+/p-}$ and PWScr$^{m+/p+}$ cultures after 1 h of treatment. The theta power of the PWScr$^{m+/p+}$ cultures decreased by 60%, whereas that of the PWScr$^{m+/p-}$ cultures decreased by 30%. **(C2)** Beta power following CCh administration. We normalized the power with respect to the basal value (indicated by the dashed line). After dividing the entire recording into 30-min intervals, we did not find a significant difference between PWScr$^{m+/p+}$ and PWScr$^{m+/p-}$. All data is presented as the mean ± SEM. Statistical analysis was performed using Tukey's post hoc test following two-way repeated-measures ANOVA (*$P < 0.05$ indicated statistical difference between genotype in the different time-points; °$P < 0.05$ indicated statistical difference within the same genotype during CCh administration with respect to the basal condition).

Paternal *Snord116* deletion alters the synchronization of activity and delays response to CCh treatment

We analyzed the high frequency range of the signal (i.e., MUA) to evaluate possible network activity defects correlated with the syndrome. First, we compared the first 2 h of the spontaneous activity highlighted in Figure 4A. PWScr$^{m+/p+}$ revealed highly synchronized activity during the basal phase, composed of network-wide bursts separated by periods of nearly complete quiescence, or asynchronous action potentials (27–29), as depicted in the raster plot of one representative experiment in Figure 4B. In contrast, PWScr$^{m+/p-}$ cultures displayed a relatively asynchronous firing pattern, as demonstrated by the following analysis. We found no significant differences by comparing the firing rate during BL, denoting a comparable starting level of activity (Fig. 4C, light blue box and light red box for PWScr$^{m+/p+}$ and PWScr$^{m+/p-}$ cultures, respectively). PWScr$^{m+/p-}$ cultures displayed more desynchronized activity than PWScr$^{m+/p+}$ resulted in a reduced burstiness index (BI) (Mann–Whitney U test; $Z = 2.18$, $P = 0.02$) (BI, Fig. 4C1) and spike time tiling coefficient (STTC; Mann–Whitney U test; $Z = 2.29$, $P = 0.01$; Fig. 4C2). The analysis of the cross-correlation of burst events (Fig. 4C3 and C4) revealed a statistically significant difference in the latency of the top 100 connections between the two groups under basal conditions (Mann–Whitney U test; $Z = -1.94$; $P = 0.049$) (Fig. 4C4). We did not find any significant difference in the C_{peak} values (Fig. 4C3).

To enable the behavior of the cultures to be compared during CCh stimulation, we normalized the results of each experiment to the mean values obtained during basal recording. In the PWScr$^{m+/p+}$ cultures (Fig. 4F, blue line), the activity level evaluated by means of the mean firing rate (MFR) increased

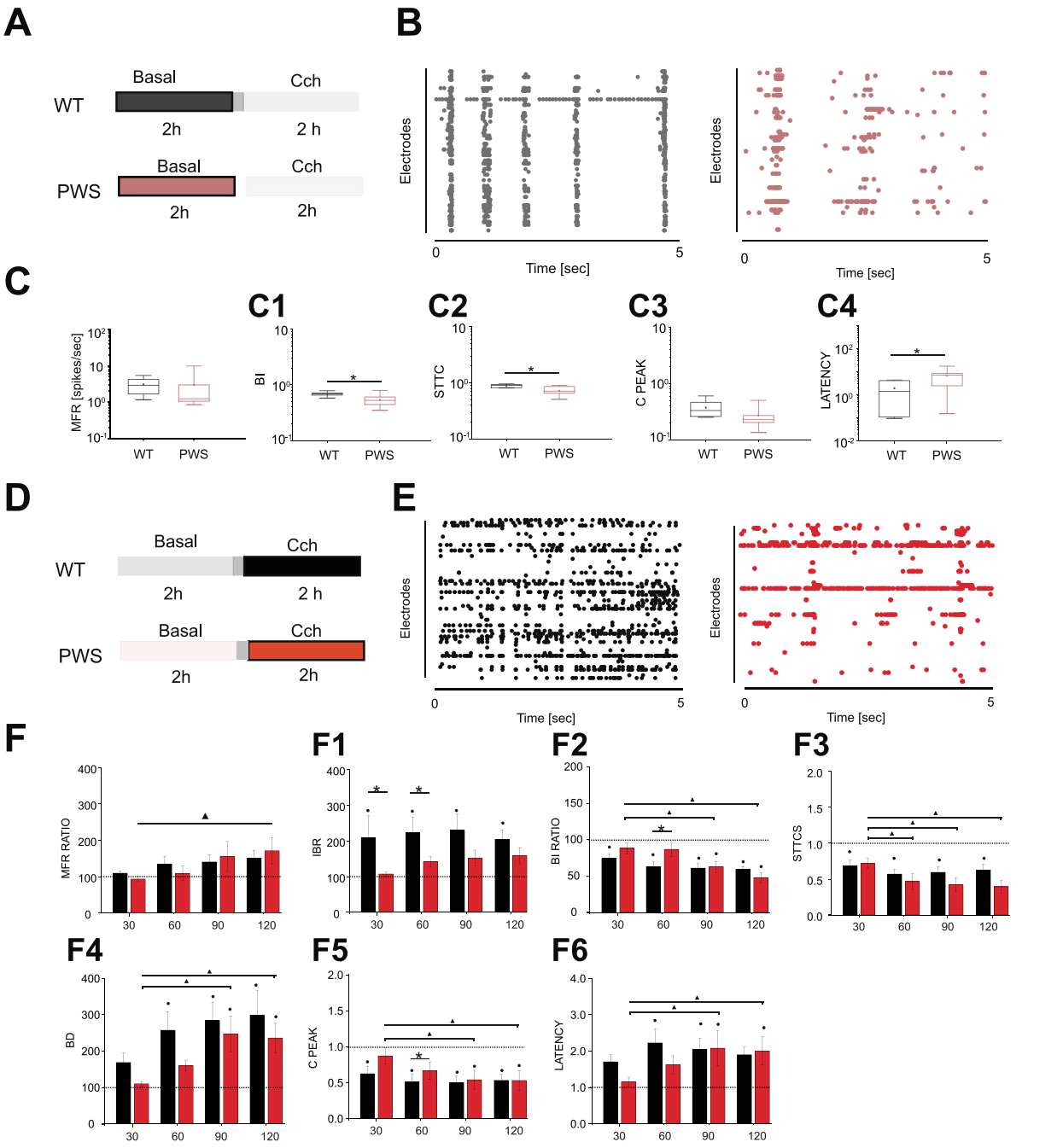

Figure 4. MEA analysis of PWScr$^{m+/p+}$ and PWScr$^{m+/p-}$ cortical cultures. (**A**) Experimental protocol adopted for the experiments. The 2 h of basal recording used in the analysis are highlighted. (**B**) 150-s raster plots of cortical cultures at DIV 18 during basal phase for PWScr $^{m+/p+}$ and PWScr $^{m+/p-}$ cultures. (**C**) Comparison of MFR in PWScr$^{m+/p+}$ (gray box, N = 6) and PWScr$^{m+/p-}$ (light red box, $n = 9$) cultures during basal phase. (**C1**) Comparison of BI in PWScr$^{m+/p+}$ (gray box plot, $n = 6$) and PWScr $^{m+/p-}$ (light red box, $n = 9$) cultures during basal phase. (**C2**) Comparison of STTC values in PWScr$^{m+/p+}$ (gray box plot, $n = 6$) and PWS (light red box, $n = 9$) cultures during basal phase. (**C3**) Comparison of the top 100 C_{peak} values calculated on burst events in PWScr$^{m+/p+}$ (gray box plot, $n = 6$) and PWScr$^{m+/p-}$ (light red box, $n = 9$) cultures during basal phase. (**C4**) Comparison of the top 100 latency value calculated on burst events in PWScr$^{m+/p+}$ (gray box plot, $n = 6$) and PWScr$^{m+/p-}$ (light red box, $n = 9$) cultures during basal phase. (**D**) Experimental protocol adopted for the experiments. The 2 h of CCh recording used in the analysis are highlighted. (**E**) 150-s raster plots of cortical cultures at DIV 18 during basal and CCh administration for PWScr$^{m+/p+}$ and PWScr$^{m+/p-}$ cultures. (**F**) Comparison of 30-min time-point of MFR in PWScr$^{m+/p+}$ (black columns, $n = 6$) and PWScr$^{m+/p-}$ (red columns, $n = 9$) cultures following CCh administration. (**F1**) Comparison of 30-min time-point of IBR in PWScr$^{m+/p+}$ (black columns, $n = 6$) and PWScr $^{m+/p-}$ (red columns, $n = 9$) cultures following CCh administration. (**F2**) Comparison of BI in PWScr $^{m+/p+}$ (black columns, $n = 6$) and PWScr $^{m+/p-}$ (red columns, $n = 9$) cultures following CCh administration. (**F3**) Comparison of the top 100 STTC values obtained for PWScr$^{m+/p+}$ (black columns, $n = 6$) and PWScr$^{m+/p-}$ (red columns, $n = 9$) cultures following CCh administration. (**F4**) Comparison of BD in PWScr$^{m+/p+}$ (black column, $n = 6$) and PWScr$^{m+/p-}$ (red column, $n = 9$) cultures following CCh administration. (**F5**) Cross-correlation analysis of burst events. Bar plot of the 100 highest C_{peak} values at each 30-min time-point. (**F6**) Bar plot of the corresponding peak latency values (L_{peak}) of the preselected 100 highest C_{peak} values. In each box plot (C4), the small square indicates the mean, the central line indicates the median and the box limits indicate the 25th and 75th percentiles. All data is presented as the mean ± SEM. Statistical analysis was performed using Tukey's post hoc test following two-way repeated-measures ANOVA (*$P < 0.05$ indicated statistical difference among the different time-points treatment (i.e. CCh 60′ and CCh 120′) within the same genotype, $P < 0.05$ indicated statistical difference within the same genotype during CCh administration with respect to the basal condition).

after CCh administration compared with the basal condition, but we did not find any significant difference. At the same time, CCh application resulted in an increased number of isolated spikes (i.e. an increased inverse burst ratio [IBR] value, Fig. 4F1) (two-way repeated-measures ANOVA; basal phase versus CCh 30′: $q = 5.87$, $P = 0.001$; basal phase versus CCh 60′: $q = 6.62$, $P < 0.001$; basal phase versus CCh 90′: $q = 7.02$, $P < 0.001$; basal phase versus CCh 120′ $q = 5.639$, $P = 0.002$) and a decrease in the BI (two-way repeated-measures ANOVA; basal phase versus CCh 30′: $q = 4.338$, $P = 0.02$; basal phase versus CCh 60′: $q = 6.21$, $P < 0.001$; basal phase versus CCh 90′: $q = 6.603$, $P < 0.001$; basal phase versus CCh 120′: $q = 6.95$, $P < 0.001$) (Fig. 4F2) and STTC (two-way repeated-measures ANOVA; basal phase versus CCh 30′: $q = 5.181$, $P = 0.005$; basal phase versus CCh 60′: $q = 7.069$, $P < 0.001$; basal phase versus CCh 90′: $q = 6.666$ $P < 0.001$; basal phase versus CCh 120′: $q = 6.125$ $P < 0.001$; Fig. 4F3) compared with the basal phase, indicating a loss of bursting activity and of synchronicity. Moreover, CCh causes a fragmentation of burst structures resulting from an increase in burst duration (BD) (Fig. 4F4) (two-way repeated-measures ANOVA; basal phase versus CCh 60′: $q = 5.142$, $P = 0.006$; basal phase versus CCh 90′: $q = 6.02$, $P < 0.001$; basal phase versus CCh 120′: $q = 6.504$, $P < 0.001$), a decrease in the peak of cross-correlation on burst events (C_{peak}, Fig. 4F5) (two-way repeated-measures ANOVA; basal phase versus CCh 30′: $q = 4.474$, $P = 0.021$; basal phase versus CCh 60′: $q = 5.805$, $P = 0.001$; basal phase versus CCh 90′: 5.938, $P = 0.001$; basal phase versus CCh 120′: $q = 5.58$, $P = 0.002$) and an increase in the latency of the top 100 connections (Lat; Fig. 4F6) (two-way repeated-measures ANOVA; basal phase versus CCh 60′: $q = 4.962$, $P = 0.008$; basal phase versus CCh 90′: 4.263, $P = 0.031$). Indeed, the relative changes of the analyzed parameters upon CCh administration in PWScr$^{m+/p+}$ cultures are consistent with the previous results obtained in cortical cultures from embryonic rats despite the different *in vitro* ages (DIVs) of the recorded cultures (26). Although the starting level of spontaneous firing was comparable between genotypes (Fig. 4C), whereas CCh had a delayed effect in PWScr$^{m+/p-}$ cultures. We found a significant difference between the first 30 min and the last 1 h of CCh administration for the MFR ratio (two-way repeated-measures ANOVA; CCh 30′ versus CCh 120′: $q = 4.783$, $P = 0.012$) (Fig. 4F). We did not find any significant difference in the IBR ratio of PWScr$^{m+/p-}$ at any time-point of 30 min (Fig. 4F1). In contrast, the BI (two-way repeated-measures ANOVA; CCh 30′ versus CCh 90′: $q = 5.37$, $P = 0.003$; CCh 30′ versus CCh 120′: $q = 8.568$, $P < 0.001$) (Fig. 4F2), STTCs (two-way repeated-measures ANOVA; CCh 30′ versus CCh 60′: $q = 5.03$, $P = 0.007$; CCh 30′ versus CCh 90′: $q = 5.934$, $P = 0.001$; CCh 30′ versus CCh 120′: $q = 6.501$, $P < 0.001$) (Fig. 4F3), BD (two-way repeated-measures ANOVA; CCh 30′ versus CCh 90′: $q = 5.544$, $P = 0.002$; CCh 30′ versus CCh 120′: $q = 5.093$, $P = 0.006$) (Fig. 4F4), C_{peak} (Fig. 4F5) (two-way repeated-measures ANOVA; CCh 30′ versus CCh 90′: $q = 4.86$, $P = 0.01$; CCh 30′ versus CCh 120′: $q = 5.008$, $P = 0.007$) and latency ratio (Fig. 4F6) (two-way repeated-measures ANOVA; CCh 30′ versus CCh 90′: $q = 4.607$, $P = 0.016$; CCh 30′ versus CCh 120′: $q = 4.244$, $P = 0.032$) showed a statistically significant difference between the time-point of 30 min and the subsequent time-points of 90 and 120 min by CCh treatment. Indeed, in contrast to PWScr$^{m+/p+}$ cultures, the above parameters showed a statistically significant difference with respect to the basal conditions starting 90 min after the administration of the drug (Fig. 4F2–F6).

When we compared the behavior of PWScr$^{m+/p+}$ and PWScr$^{m+/p-}$, we observed a higher increase in the IBR values for PWScr$^{m+/p+}$ than for PWScr$^{m+/p-}$ in the first hour by the CCh administration (Fig. 5F1) (two-way repeated-measures ANOVA; CCh 30′: $q = 3.767$, $P = 0.013$; CCh 60′: $q = 2.986$, $P = 0.045$). At the same time, the BI ratio (Fig. 4F2) (two-way repeated-measures ANOVA; CCh 60′: $q = 3.37$, $P = 0.02$) and the C_{peak} ratio (Fig. 4F5) (two-way repeated-measures ANOVA; CCh 60′: $q = 3.10$, $P = 0.03$) showed lower values for PWScr$^{m+/p-}$ than for PWScr$^{m+/p+}$ after 1 h of treatment. Instead, at the same time-point, the BD ratio revealed higher values for PWScr$^{m+/p+}$ than for PWScr$^{m+/p-}$ (Fig. 4F4). Therefore, paternal *Snord116* deletion causes alterations in the synchronization level of activity and a delayed response to CCh treatment. All the statistical details from the multiple pairwise comparisons are available in Supplementary Material, Table S6.

Paternal *Snord116* deletion alters the expression of IEGs *in vivo* and *in vitro*

We explored the impact of *Snord116* on the expression of selected IEG in the cortex, as they represent an important target of both neuronal responses and sleep homeostasis. In the *in vivo* experiment, IEG expression was investigated in the frontal cortex (FC) and parietal cortex (PC) of adult mice (15–18 weeks old) sacrificed at ZT6 and 1 h after 6 h of sleep deprivation (SD). We observed that at ZT6, which constitutes the BL condition, *Bdnf* expression was significantly reduced in the PWScr$^{m+/p-}$ mice compared with the control (PWScr$^{m+/p+}$ 1 ± 0.12 versus PWScr$^{m+/p-}$ 0.46 ± 0.07, $t(8) = 3.73$, $P = 0.005$; Supplementary Material, Fig. S4A) in the PC. This increase in the *Bdnf* level was also observed in the PC of mutant mice (PWScr$^{m+/p+}$ 1 ± 0.12 versus PWScr$^{m+/p-}$ 0.62 ± 0.06, $t(8) = 2.68$, $P = 0.02$; Supplementary Material, Fig. S4A). Moreover, in the PC, a significant reduction in *Cfos* (PWScr$^{m+/p+}$ 1 ± 0.37 versus PWScr$^{m+/p-}$ 0.09 ± 0.03, $t(8) = 2.38$, $P = 0.04$; Supplementary Material, Fig. S4A) and *Arc* (PWScr$^{m+/p+}$ 1 ± 0.19 versus PWScr$^{m+/p-}$ 0.37 ± 0.13, $t(8) = 2.64$, $P = 0.02$; Supplementary Material, Fig. S4A) genes was also observed. We noticed that, 1 h after 6 h of SD, the expression levels of all investigated IEGs were significantly reduced in the mutant mice compared with control mice (Fig. 5; see Supplementary Material, Table S2 for statistical analysis). Conversely, the expression levels of all investigated IEGs were, as expected, significantly increased compared with the BL value (ZT6, non-SD mice) in the PWScr$^{m+/p+}$ mice (21) (Fig. 5; see Supplementary Material, Table S3 for statistical analysis). The same scenario was observed for the expression of IEGs in the PC of the mutant mice (Supplementary Material, Fig. S4A; see Supplementary Material, Table S3 for statistical analysis).

Subsequently, the alteration in cortical IEG expression observed in living PWScr$^{m+/p-}$ mice 1 h after SD was investigated to determine whether it is also reflected in the embryonic cortical neurons. For the *in vitro* analyses, cortical cultures were stimulated with 20 μm of CCh, and RNA was extracted 1 h later, which resembled the *in vivo* SD condition. Conversely, the ZT6 treatment in the *in vivo* experiment mirrors the cell culture stimulated with water (BL). In primary cell cultures at BL, the only IEG whose expression was significantly different between the two genotypes was *Per2*. In this condition, *Per2* was found to be significantly higher in the PWScr$^{m+/p-}$ cultures than in the control cultures (PWScr$^{m+/p+}$ 1 ± 0.31 versus PWScr$^{m+/p-}$ 19 ± 2.6, $t(8) = 7.01$, $P = 0.0001$; Supplementary Material, Fig. S4B). It was also observed that, 1 h after CCh treatment, cells displayed the same alterations in IEG expression that were observed in the *in vivo* experiment. Specifically, it was observed that all IEG expression levels were significantly lower in the PWScr$^{m+/p-}$ mice than in the control mice (Fig. 5; see

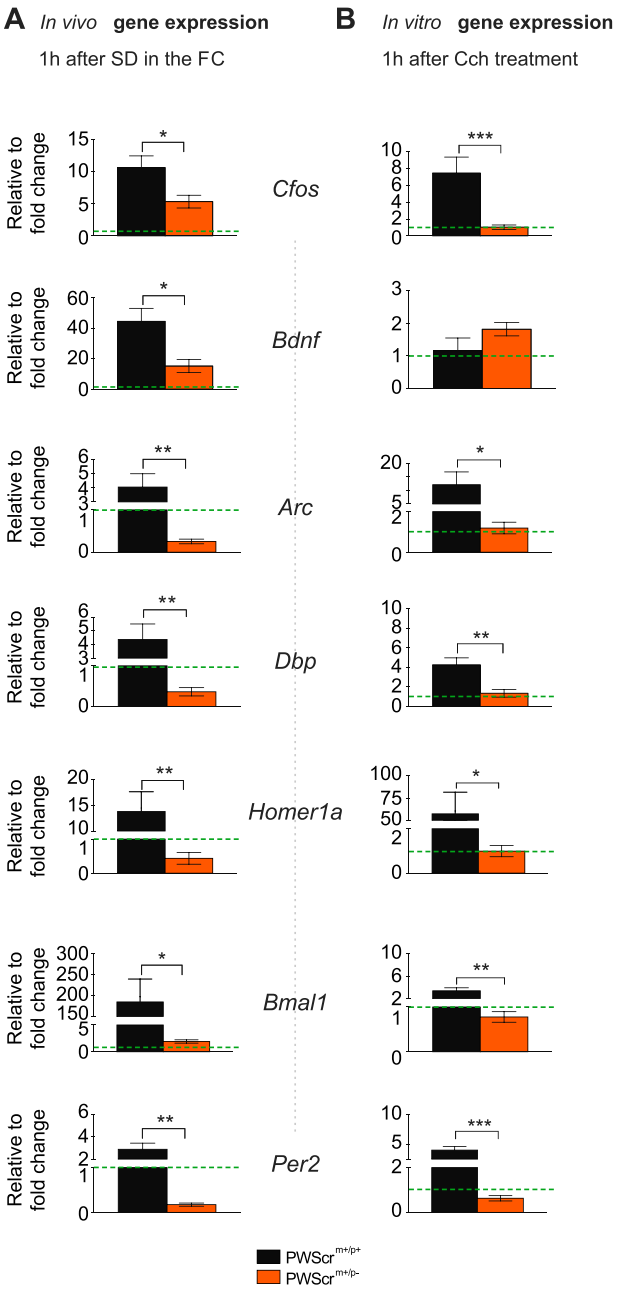

Figure 5. Paternal *Snord116* deletion alters the IEGs *in vivo* and *in vitro*. (**A**) IEG gene expression analysis was performed in PWScr$^{m+/p+}$ ($n = 10$ in black) and PWScr$^{m+/p-}$ mice ($n = 10$ in red). Mice were sacrificed after 6 h of sleep deprivation and 1 h of rebound. Values expressed are relative to wild-type control average ± SEM. Green line shows the baseline level. $^{**}P < 0.01$; $^{***}P < 0.001$. (**B**) IEG gene expression analysis was performed in embryonic cortical neurons obtained from PWScr$^{m+/p+}$ ($n = 5$ in black) and PWScr$^{m+/p-}$ mice ($n = 5$ in red). Cells were collected after 1 h of CCh treatment. $P < 0.05$; $^{**}P < 0.01$; $^{***}P < 0.001$. IEG investigated: *Fos* Proto-oncogene, AP-1 transcription factor subunit (*C-fos*); brain-derived neurotrophic factor (*Bdnf*); activity regulated cytoskeleton associated protein (*Arc*); D-box binding PAR BZIP transcription factor (*Dbp*); Homer scaffold protein 1 (*Homer1a*); brain and muscle ARNT-like 1 (*Bmal1* also named as aryl hydrocarbon receptor nuclear translocator-like protein 1 (*Arntl*); period circadian regulator 2 (*Per2*).

Supplementary Material, Table S4 for statistical analysis). In contrast, PWScr$^{m+/p+}$ mice showed significantly increased IEG expression after CCh treatments, as observed in the *in vivo* experiments (Fig. 5; see Supplementary Material, Table S4 for statistical analysis). Interestingly, only *Bdnf*, which is not an IEG but is involved in the plasticity mechanisms, did not undergo a change in expression in cultured cortical neurons 1 h after CCh (Fig. 5; see Supplementary Material, Table S4 for statistical analysis), while in living mice, the expression of this gene was significantly altered before and after SD.

Overall, these *in vivo* and *in vitro* results show that IEG expression in the cortex is significantly affected by the loss of the *Snord116* gene. Additionally, it was observed herein that the wake-like (CCh treatment versus SD mice) and sleep-like states (water treatment versus ZT6 mice) *in vitro* underwent changes in gene expression that resembled those in the cerebral cortex of living animals.

Discussion

The results of this study confirm that the *Snord116* gene significantly affects REM sleep occurrence and its regulation. Sleep spindle properties were found, for the first time, to be altered in the PWScr$^{m+/p-}$ mice, while their numbers were unchanged between the two genotypes, suggesting dysfunctions in the TC relay neurons where sleep spindles are amplified and not in the thalamic reticular nucleus (TRN) where they are generated. Moreover, we also described a previously unreported form of intrinsic cortex dysfunction observed in primary cortical neurons obtained from PWScr$^{m+/p-}$ mice, reinforcing our results obtained on sleep spindles. Next, the electrophysiological and molecular changes that we observed in primary cortical neurons resemble the same sleep phenotypes and transcriptional changes observed in living mice.

Mice carrying a paternal deletion of the *Snord116* and *Ipw* genes display REM sleep dysregulation, suggesting that also *Ipw* may contribute to effect that we reported. Specifically, we observed a pronounced increase in REM sleep during the dark period, when mice are most active, and may resemble the EDS observed in humans PWS (6). This dysregulation of REM sleep is in agreement with our previous report (14), which describes an increase of REM sleep in both, in mice having the paternal deletion of the *Snord116* gene and in two PWS subjects carrying the small deletion embracing only the *Snord116* gene.

Since REM sleep is precisely regulated in terms of its duration and NREM is substantially regulated in terms of intensity (30,31), we decided to analyze the succession of REM sleep episodes and the period of time intervening between the end of one REM sleep episode and the beginning of the next (RSI). We found that RSI followed a bimodal distribution characterized by short and long periods. The presence of a bimodal distribution has already been described (32) in many species, such as rats (33), cats (34) and humans (35), but, at the best of our knowledge, no data is yet available on the RSI distribution in mice. For the first time, our data revealed a bimodal RSI distribution in mice, with the minimum frequency at 55 s, while in rats, the minimum between the two peaks has been identified at 3 min (32). A bimodal distribution of RSI was observed in both genotypes of mice. However, mutant mice showed a significant increase in short RSI. Short RSI has been described as an indicator of the capacity to produce REM sleep in accordance to the homeostatic drive under favorable ambient conditions and associated with the capacity to produce REM sleep proportionally to the homeostatic drive under favorable ambient conditions (32,36). Indeed, the amount of REM sleep with short RSIs has been shown: (i) to be increased during a REM sleep rebound in proportion to the degree of previous REM deprivation induced by low ambient temperature (37); (ii) to be depressed when animals

are kept under an uncomfortable ambient condition, such as during the exposure to a low Ta (32), and concomitantly with a reduced capacity of cyclic adenosine monophosphate accumulation at hypothalamic-preoptic level (38,39). This observation may reflect a strengthened drive for REM sleep and/or a distorted and more favorable perception of the ambient conditions, in terms of the thermal comfort, in the mutant mice. Therefore, since sleep propensity also affects the NREM–REM cycle, we also assessed the number of these cycles over the 24 h of the BL in both genotypes of mice. As expected, mutant mice presented a significant increase in the NREM–REM cycle (~2–5 min) (23) compared with the control group, suggesting, once again, that the mutant mice have a strong tendency to fall asleep easily. Overall, this data implies that the loss of *Snord116* significantly compromised sleep macrostructure, mainly affecting REM sleep.

We found that PWScr$^{m+/p-}$ mice showed alterations in REM sleep without affecting NREM sleep. An exception, however, was found in the sleep spindles, hallmarks of NREM sleep that reflect the activity of complementary TC circuits. The TRN have a propensity to trigger spindle oscillations and fire in bursts at every cycle, acting as pacemaker cells. TC cells receive inhibitory synaptic input from the TRN, produce rhythmic bursts and contribute to initiate or amplify spindle oscillations (40,41). Here, we show that the duration, amplitude and intraspindle frequency of sleep spindles are significantly altered in PWScr$^{m+/p-}$ mice, while their numbers are unchanged between the two genotypes. Notably the intraspindle frequency is an important parameter characterizing intrinsic properties of TC network activity (42,43). This data suggests that TRN/thalamus circuits to these intrathalamic circuits may probably not affected in the mutant mice, while, an impairment of TC amplification may explain the alterations of sleep spindles properties. Since it has been shown that sleep spindles facilitate neuroplasticity and support learning, memory consolidation and intellectual performance (44), and since sleep spindle alterations have been documented in children with neurodevelopmental disorders (44,45), we speculate that the neurodevelopmental and cognitive alterations observed in these mice (46) may also be associated with altered TC input. Thus, we believe that sleep spindle alterations may either reflect the severity of the underlying disorder or directly exacerbate the severity of impairments. Evidence also indicates that alterations in sleep spindle properties have a very early association with an increased risk of cognitive impairment (47); our results imply that sleep spindles may also represent reliable sleep EEG biomarkers associated with PWS disorder, although a better characterization of these findings in PWS subjects is needed.

Additionally, we observed that PWScr$^{m+/p-}$ mice have dysregulated norepinephrine levels in the CSF collected at the beginning of the dark period. Norepinephrine is a neurotransmitter and is important for maintaining normal sleep states, and dysregulated norepinephrine signaling is responsible for cataplexy attacks, which, together with narcolepsy, represent common features of PWS (48). Thus, the activity of norepinephrine neurons in the locus coeruleus is important in modulating cortical activity during NREM sleep (49). Norepinephrine not only influences general arousal but also affects locomotor activity. Indeed, it has been observed that intraventricular infusion of norepinephrine increases motor activity (50). Interestingly, we observed that norepinephrine was significantly higher in the mutant mice than in the controls, suggesting that norepinephrine may also have a role in controlling motor activity in these mice. Indeed, in our mutant mice, we observed a significant increase in physical activity during the dark period. However, these results are inconsistent with PWS human data, which instead shows a reduction of the physical activity in PWS subjects. This data suggests that the complexity of the genetic background in humans compared with mice may mostly affect the metabolic aspect accounting for one of the main symptoms of the PWS. Additionally, this data also implies further experiments to replicate and clarify our findings related to either the increase in the physical activity of PWS mutant mice or the alteration of norepinephrine that may affect the sleep–wake cycle and locomotor activity.

Our data implies a dysfunction of TC amplification, manifested by the altered sleep spindles properties not affecting their numbers observed in the mutant mice. Based on these results, we investigated whether cortical neurons isolated from TC projections showed an altered intrinsic mechanism of sleep comparable to the sleep endophenotypes observed in living mice. To address this question, we used an *in vitro* model. Previous studies have demonstrated that embryonic cortical neurons on MEA are able to recapitulate some essential features of sleep in a controllable way (21,26,51). Here, we treated cortical cultures with CCh to change the synchronized default sleep-like state, characterized by slow-wave oscillations typical of NREM sleep, into a theta-predominant state, which is typical of REM sleep. Because of this EEG feature of REM, the shorthand definition of REM sleep is a highly activated brain in a paralyzed body (52). The LFP analysis of MEA cortical neurons revealed abnormalities in the theta waves in the PWScr$^{m+/p-}$ neurons similar to those observed in living mice. CCh administration caused evident desynchronization of the activity of both genotypes, but mutant cultures showed different response profiles after CCh treatment compared with control cultures. In particular, PWScr$^{m+/p-}$ cultures displayed less reactivity in response to the treatment, especially during the first hour. Overall, these results suggested that PWS cultures displayed alterations in neuronal activity patterns during spontaneous activity and when external stimulation was applied. Additionally, the analysis of the MEA frequency range revealed aberrant neuronal network activity patterns. In particular, PWScr$^{m+/p-}$ cultures displayed less synchronized activity than control cultures did, as indicated by their lower BI and STTCs. Moreover, the analysis of the cross-correlation during the basal period showed shorter latencies for PWScr$^{m+/p+}$ cultures than for PWScr$^{m+/p-}$ cultures. Taken together, this data implies that *Snord116* may either directly influence the neuronal synchronization of cortical neurons or affect it indirectly via norepinephrine, which we found to be altered in our study in living mice. Indeed, norepinephrine is a neurotransmitter that decreases network synchrony both *in vivo* (53,54) and *in vitro* (54), consistent with our results, in which PWScr$^{m+/p-}$ cultures showed an increased level of this neurotransmitter that may be responsible for the increased desynchronization level of activity in the MEA recording.

Finally, we also assessed the expression of IEGs in both *in vitro* and *in vivo* models, and we observed that our *in vitro* model exactly recapitulates the transcriptional alteration observed in living mice. This finding also suggests that cortical cultures coupled to MEA represent a promising tool to identify novel therapeutic targets, such as sleep feature alterations and network synchronization defects. Moreover, this data suggests, in agreement with a recent publication (55), that the *Snord116* gene affects the transcriptional profiles of circadian genes in the cortex (*Per2* and *Bmal1*), which are involved in development outside the suprachiasmatic nucleus and contribute to brain plasticity (56). Indeed, we also found that the PWScr$^{m+/p-}$ mice had low levels of *Bdnf* mRNA, which is important in the regulation of synapses and the plasticity process. This latter

evidence may pave the way for new interventional approaches for PWS by using TrkB agonists or by using compounds that increase the brain-derived neurotrophic factor (BDNF) level (57).

Overall, our results suggest that *Snord116* is important in controlling REM sleep. Additionally, here, we provide evidence supporting the role of *Snord116* in regulating TC/cortical neuronal activity, opening avenues for new interventions in PWS. The dysregulation of sleep spindles in our mutant mice raises the possibility that this phenomenon can be a clinically useful marker to assess PWS symptoms in humans.

Materials and Methods

In vivo study

Animals. Animal procedures were performed at the Istituto Italiano di Tecnologia, Genova, Italy and were approved by the Animal Research Committee and the Veterinary Office of Italy. All efforts were made to minimize the number of animals used, as well as any pain and discomfort, according to the principles of the three Rs (replacement, reduction and refinement) (58).

Mice carrying a paternal deletion of the *Snord116* gene and IPW exons A1/A2 B (59) ($PWScr^{m+/p-}$) were used in this study, along with wild-type mice ($PWScr^{m+/p+}$). In order to maintain the colony, patrilineal descendants of the original transgenic mice were bred on a C57BL/6 J background. For the genotyping protocol, see Supplementary Materials.

All animals used in this study were housed under controlled temperature conditions ($22 \pm 1^{\circ}C$ as room temperature) on a 12 h:12 h light/dark cycle (lights on 07:00–19:00). Food (standard chow diet) and water were provided *ad libitum*.

Experimental design. For the study, male mice with paternally inherited *Snord116* deletions ($PWScr^{m+/p-}$) and wild-type littermate control mice ($PWScr^{m+/p+}$) aged 15–18 weeks were used.

To investigate the impact of *Snord116* in the sleep architecture, we made continuous recordings by EEG combined with electromyography (EMG) for 24 h (12 h:12 h light/dark cycle, Fig. 1A). Subsequently, we investigated changes in spindle properties at specific time-points across the sleep–wake cycle. Specifically, EEG/EMG recordings were made for 2 h at two different time-points as the BL condition (B1 and B2; Fig. 1D) to investigate spindle properties related to (i) circadian variation (switch from light to dark periods) and (ii) homeostatic variation (low and high sleep pressure). Thus, we investigated the frequency of sleep spindles and their properties in response to perturbation of sleep by performing 6 h of total SD. EEG/EMG recordings were made over the first hour of the rebound period (RB, Fig. 1D) following 6 h of SD (RB1) and at two other time-points over the 18 h recovery period (RB2 and RB3, Fig. 1D).

In vivo SD protocol. Total SD was performed by gentle handling techniques, consisting of introducing novel objects into the cage, knocking or shaking the cage whenever animals are inactive or display behaviors associated with sleep (asleep account for inactivity, twitching or if mice eyes are closed). Animals were subjected to SD during the last 6 h of the light period, which the sleep pressure is high. Animals were visual inspected throughout all SD procedure.

EEG/EMG electrode implantation. A total of 28 male mice were used for the *in vivo* sleep study ($n = 14$ $PWScr^{m+/p-}$ and $n = 14$ $PWScr^{m+/p+}$ mice). Notably only male mice were used since it has been shown that gonadal hormones may interfere with sleep distribution, and intensity (60). Each mouse was anaesthetized using 1.5–2.5% isoflurane in oxygen and surgically implanted with a telemetric transmitter (volume, 1.9 cm^3; total weight, 3.9 g; TL11M2-F20-EET; DSI, Saint Paul, MN, USA) connected to electrodes for continuous EEG/EMG recording to assess the sleep–wake cycle. A wireless EEG transmitter/receiver was subcutaneously implanted. EEG wire electrodes were implanted epidurally over the right FC (coordinates: 2 mm posterior to bregma and 2 mm lateral to the midline, in the right frontal part of the skull) and the right PC (coordinates: 3 mm anterior to lambda and 2 mm lateral to the midline, in the right parietal part of the skull). EMG was recorded with two stainless steel wires inserted bilaterally into the neck muscles ~5 mm apart and sutured in place (Fig. 1A). Following surgery, all animals received paracetamol (200 mg/kg orally once a day; Tempra) and enrofloxacin (10 mg/kg subcutaneously once a day; Baytril) for 2 days after surgery. The animals were housed individually in their home cages for a recovery period of 7 days, after which EEG/EGM signals were recorded continuously for each mouse.

EEG/EMG analysis. Cortical EEG and EMG signals were recorded using Dataquest A.R.T. (Data Science International). Activity data measured only relative movement, which is dependent on the orientation and distance between the transmitter and receiver. Signals were digitized at a sampling rate of 500 Hz with a filter cut-off of 50 Hz. EEG signals were filtered at 0.3 Hz (low-pass filter) and 0.1 kHz (high-pass filter), respectively. The polysomnographic recordings were visually scored offline using SleepSign software (Kissei Comtec Co. Ltd, Japan) in 4-s epochs to identify the wakefulness (W), NREM sleep (NR) or REM sleep (R) stages as previously described (61,62). Scoring was performed by a single observer who was blinded to the group assignments of the mice. EEG epochs determined to have artefacts (interference caused by scratching, movement, eating or drinking) were excluded from the analysis. Artefacts comprised <5–8% of all recordings used for analysis.

The numbers of epochs spent in wakefulness, NREM and REM were determined for a 24-h circadian period, across the light and dark phases (L:D = 12:12). The amount of time spent in each stage was established by the count of the epoch type (W, NR or R) and averaged over 2-h periods. The spectral characteristics of the EEG data was further analyzed. EEG power density for delta (0.5–4 Hz) frequencies in NREM sleep was computed over the 24 h of recording time. The power of each 0.5 Hz bin was first averaged across the sleep stages individually and then normalized by calculating the relative duration of each bin from the total power (0–20 Hz) for each individual animal.

A two-way repeated-measures ANOVA with factors of group × time was used for the statistical analysis of 2-h averaged time-course changes in the quantity of each sleep stage (W, NREM and REM) and for physical activity. The statistical analysis of the cumulative amounts of W, NREM and REM over the dark and light periods between genotypes was carried out with a two-tailed *t*-test. A two-way repeated-measures ANOVA with factors of group × frequency (Hz) was used for the statistical analysis of EEG power for NREM sleep over the 24-h recording period.

REM sleep characterization. Additional analyses were performed to characterize the REM sleep alterations observed in the $PWScr^{m+/p-}$ mice. In particular, a more detailed analysis of REM sleep was carried out according to the partition of REM sleep episodes into single and sequential episodes, which has

originally been proposed for rats (37). First, the RSIs, given by the sum of the time spent in wakefulness and in NREM sleep between two REM sleep episodes, were calculated. Here, the bimodal distribution of RSI length was determined using a kernel density estimation mathematical model, and single REM sleep episodes and sequential REM sleep episodes were discriminated (Supplementary Material, Fig. S1). A single RSI is defined as the time interval from the end of one REM sleep episode to the beginning of the next episode. The criteria used to discriminate the long and the short RSIs were: long RSIs >60 s each, while sequential REM sleep episodes are those that are separated by short RSIs ≤ 60 s each (Fig. 1C) as previously described (37).

Second, the REM–NREM cycle, which is defined as the interval between the onset of consecutive REM episodes, was assessed. The following criteria were used: 8 s was the minimum length of a REM sleep episode; and cycles that were longer than 30 min were excluded from the analysis, since it has been already documented in mouse studies that the cycle length is ∼2–5 min (23). An unpaired *t*-test was used to assess differences between short and long RSIs and differences in the number of REM–NREM sleep cycles.

Sleep spindle properties. Individual sleep spindles were detected using a threshold-based spindle detection method. Briefly, the algorithm estimates the energy of EEG signal within 9–16 Hz range, and then applies a threshold (3 SD + Mean) to detect candidate spindles. A lower threshold (1 SD + Mean) is then applied to find start and end points of the candidate spindles. Afterward, several properties of the detected spindles are calculated automatically, such as density, duration, central frequency (i.e. average number of peaks for each spindle expressed in peaks/seconds, Hz), peak-to-peak amplitude, and symmetric measure.

Neurochemical analysis. Neurochemical analysis was performed in PWScr$^{m+/p-}$ mice ($n=5$) and PWScr$^{m+/p+}$ mice ($n=5$). Mice were anaesthetized with isoflurane at the beginning of the dark period to collect CSF. We decided to collect samples at this time-point because REM sleep alterations were observed at this stage. CSF was sampled as previously described (63). Mice were anaesthetized using 1.5–2.5% isoflurane in oxygen and placed on a platform, and the arachnoid membrane covering the cisterna magna was punctured. The positive flow pressure allows the collection of CSF using a glass micropipette with a narrow tip. Three to eight microliters of CSF per mouse was collected and stored at −80°C in polypropylene tubes.

CSF preparation for ultrahigh-performance liquid chromatography-tandem mass spectrometry. Eighteen microliters of a solution containing 1 µM each of Glu-d5 and GABA-d6 and 50 nM His-d4 in aqueous 0.1% formic acid was added to 2 µL of each thawed sample of CSF and then vortexed and centrifuged for 10 minutes at 14000 rpm. The resulting supernatants were moved to glass vials for injection. Calibration standards were prepared by spiking artificial CSF (150 mM Na, 3 mM K, 1.4 mM Ca, 0.8 mM Mg, 1 mM P, 155 mM Cl, 10 mM glucose, 0.5 mg/mL albumin) with stock standard solutions. These calibrators were further diluted 1:10 with the internal standard solution, vortexed and centrifuged before injection.

Ultrahigh-performance liquid chromatography-tandem mass spectrometry. Chromatographic separation was performed with an Acquity UPLC system (Waters, Milford, MA, USA) using an ACE C18-Ar column (2-µm particle size, 2.1 × 150 mm (purchased from Advanced Chromatography Technologies Ltd, Aberdeen, Scotland, UK). Separation was carried out at a flow rate of 0.5 ml/min. The eluents were as follows: A, aqueous 0.1% formic acid with 5 mM *n*-perfluoropentanoic acid; B, acetonitrile with 0.1% formic acid. The gradient used starts with 1 min at 1% B, increasing linearly from 1 to 50% B in 2.5 min, and then remaining at 50% B for 30 s before the column was equilibrated with the initial conditions for 2 additional minutes, adding up to a run time of 6 min. The column and autosampler temperatures were set to 45 and 10°C, respectively. The injection volume was set to 4 µl. Analysis was performed on a XEVO TQ-S triple quadrupole mass spectrometer (Waters) equipped with an electrospray source operated in positive mode. Nitrogen was used as the desolvation (800 L/h, 450°C) and collision gas. Data was acquired in the multiple reaction monitoring mode, with the settings of the precursors, fragments, cone voltages and collision energies for each compound as indicated in Supplementary Material, Table S1. Waters MassLynx 4.1 and TargetLynx 4.1 software were used for data acquisition and processing, respectively. A paired *t*-test was used to compare the levels of each neurotransmitter between the two genotypes.

In vitro study

Cell culture. Cortical cultures were prepared from embryonic mice at gestational day 18 (E18). The hippocampi of four to five embryos were dissected out from the brain and dissociated first by enzymatic digestion in trypsin solution 0.125% (25–30 min at 37°C) and subsequently by mechanical dissociation with a fire-polished pipette. The resulting tissue was resuspended in neurobasal medium supplemented with 2% B27, 1% glutamax-1, 1% Pen-Strep solution and 10% fetal bovine serum (Invitrogen, Garlsbad, CA, USA), at the final concentration of 75 000 cells/µl. We placed a 50-µl drop onto the MEA recording area previously coated with borate buffer and poly-L-lysine to promote cell adhesion (final density ∼1200 cells/mm^2).

We recorded the activity of neuronal networks at 19 ± 1 days *in vitro* (DIV; mean ± SD), as already described (26), in mice carrying a paternal deletion of the *Snord116* gene (PWScr$^{m+/p-}$) (59) and in wild-type mice (PWScr$^{m+/p+}$).

Experimental protocol. We recorded the spontaneous activity in nine cultures from PWScr$^{m+/p-}$ mice and six from PWScr$^{m+/p+}$ mice for 2 h in culture solution as the BL condition. Then, cells were recorded continuously for 2 h following the administration of CCh (Sigma-Aldrich, 20 µM).

MEA recordings. Planar microelectrodes were arranged in an 8 × 8 layout, excluding corners and one reference electrode, for a total of 59 round planar TiN/SiN recording electrodes (30 µm diameter; 200 µm center-to-center interelectrode distance). The activity of all cultures was recorded by means of the MEA60 System (MCS). The signal from each channel was sampled at 10 kHz and amplified using an MCS amplifier with a frequency band of 1–3 kHz. Each recorded channel was acquired through the data acquisition card and monitored online through MC_Rack software (MCS). In order to reduce thermal stress on the cells during the experiment, the MEAs were kept at 37°C by means of a controlled thermostat (MCS) and covered with polydimethylsiloxane caps to prevent evaporation and changes in osmolality.

Data analysis and statistics. Starting from the raw data (i.e. the wide-band signal), we used a dual process to analyze both MUA

($f > 300$ Hz) and LFPs ($f < 300$ Hz). To capture only MUA activity, we high pass filtered the raw signal. When spikes (i.e. single over-threshold peaks) and bursts (i.e. groups of tightly packed spikes) were detected in the MUA recordings, we computed the following parameters for each channel: MFR (spikes/s), mean bursting rate (bursts/min), IBR (percentage of spikes outside the burst), BI (an index of the burstiness level of the network), BD (ms), mean frequency intraburst (spikes/s), interburst interval (ms) and STTC. Finally, we computed the cross-correlation between each pair of burst trains recorded from active channels (i.e. with MFR > 0.05 spikes/s). For each channel, we considered only the first spike for each burst (i.e. the burst event), and we computed the cross-correlation function that represents the probability of observing a burst in one channel i at time $t+\tau$ ($\tau = 3$ ms) given that there is a burst in a second channel $i+1$ at time t. To quantify the strength of the correlation between each pair of electrodes, we evaluated the correlation peak (C_{peak}). We selected only the first 100 C_{peak} values to identify only the most significant correlations. Finally, we analyzed the latency from the peak (L_{peak}) and considered the corresponding peak latency values of the preselected 100 strongest C_{peak} values (64).

To select the LFP components, we low-pass filtered the raw data between 1 and 300 Hz. We then computed the power spectral density of the decimated signal (sampling frequency 1 kHz) (μV^2/Hz) using the Welch method (windows = 5 s, overlap = 50%). We considered only the lower frequency bands of the signal; these bands, particularly the delta (0.5–4 Hz), theta (4–11 Hz) and beta (11–30 Hz) bands (26), are of particular interest in the study of the sleep–wake cycle. To characterize the LFP, we calculated the power in each of those frequency bands.

Measurement of *in vitro* and *in vivo* gene expression by real-time quantitative PCR

Total RNA was extracted from mouse cortices and from cortical cultures to assess the changes in distinct classes of genes that have already been shown to be differentially expressed during sleep and wakefulness (21,65–67). These genes are IEGs and clock genes (*Cfos; Arc; Homer1a, Dpb, Bmal1 and Per2*). The *Bdnf* gene, which is involved in neuroplasticity and responds rapidly to SD (68), was also investigated. RNA was extracted from the cortex of 10 male PWScr$^{m+/p-}$ mice ($n = 5$) and PWScr$^{m+/p+}$ mice ($n = 5$). Mice were sacrificed by cervical dislocation at two different time-points: (i) 6 h after the onset of the light period as a BL value (ZT6), before which the mice were kept undisturbed in their home cages and (ii) 1 h after 6 h of total SD. The latter time-point was used because in the *in vitro* experiments, gene expression analysis was performed 1 h after CCh treatment. The effect of CCh resembles that of SD. Total RNA was isolated separately from the FC and PC with TRIzol (Life Technologies) according to the manufacturer's instructions (69). Primary cortical neurons were treated at DIV 20 with 20 µM CCh for 1 h. Then, neurons were washed three times with ice-cold phosphate-buffered saline solution and lysed with 300 µl of TRIzol. All RNA concentrations were then determined by a NanoDrop 2000c spectrophotometer. Complementary DNA was reverse transcribed from up to 2 mg of total RNA using a high-capacity RNA-to-cDNA kit (Invitrogen) and then analyzed with SYBR GREEN qPCR mix. Reactions were performed in three technical replicates using an AB 7900HT fast real-time PCR system (Applied Biosystems). The relative quantification of expression levels was performed using a previously described ΔΔCT calculation method (62). *Gapdh* was used as a reference gene. The specific primer pairs used for the analysis were designed using Primer3 (Supplementary Material, Table S2). An unpaired *t*-test was used to compare differences between the genes investigated in the two genotypes.

Statistical analysis

The normality of the distribution of values was tested with the Kolmogorov–Smirnov test. Data is presented as the mean ± SEM. As detailed above for the *in vivo* experiment, most data were analyzed using two-way ANOVA and Student's *t*-test as appropriate for the experimental design. If the *P* values reached statistical significance, Bonferroni adjustment was further applied for post hoc analysis. For the sleep analysis, Phenopy was used (70), while GraphPad Prism6 (GraphPad Prism Software, Inc.) was used for statistical analysis. Type I error (α) was set at 0.05 ($P < 0.05$).

For MEA recordings, belonging to the *in vitro* experiment, data was analyzed using two-way repeated-measures ANOVA (factors = genotype × treatment) followed by Tukey's post hoc test. SigmaPlot software (Systat Software Inc.) was used for statistical analysis to compare data from two different populations, we performed the Mann–Whitney U test when data was not normally distributed.

Supplementary Material

Supplementary Material is available at *HMG* online.

Funding

A.A. and M.E.B.A. received funding from the European Union's Horizon 2020 Research and Innovation Programme under grant agreements No. 696656: Graphene Flagship, Core 1 and No. 785219: Graphene Flagship, Core 2.

Conflict of Interest statement: None declared.

References

1. Gunay-Aygun, M., Schwartz, S., Heeger, S., O'Riordan, M.A. and Cassidy, S.B. (2001) The changing purpose of Prader–Willi syndrome clinical diagnostic criteria and proposed revised criteria. *Pediatrics*, **108**, E92.
2. Williams, K., Scheimann, A., Sutton, V., Hayslett, E. and Glaze, D.G. (2008) Sleepiness and sleep disordered breathing in Prader–Willi syndrome: relationship to genotype, growth hormone therapy, and body composition. *J. Clin. Sleep Med.*, **4**, 111–118.
3. Tauber, M., Thuilleaux, D. and Bieth, E. (2015) Prader–Willi syndrome in 2015. *Med. Sci. (Paris)*, **31**, 853–860.
4. Holland, A.J., Treasure, J., Coskeran, P. and Dallow, J. (1995) Characteristics of the eating disorder in Prader–Willi syndrome: implications for treatment. *JIDR*, **39**, 373–381.
5. Helbing-Zwanenburg, B., Kamphuisen, H.A. and Mourtazaev, M.S. (1993) The origin of excessive daytime sleepiness in the Prader–Willi syndrome. *JIDR*, **37**, 533–541.
6. Camfferman, D., McEvoy, R.D., O'Donoghue, F. and Lushington, K. (2008) Prader–Willi syndrome and excessive daytime sleepiness. *Sleep Med. Rev.*, **12**, 65–75.
7. Vgontzas, A.N., Bixler, E.O., Kales, A., Centurione, A., Rogan, P.K., Mascari, M. and Vela-Bueno, A. (1996) Daytime sleepiness and REM abnormalities in Prader–Willi syndrome: evidence of generalized hypoarousal. *Int. J. Neurosci.*, **87**, 127–139.

8. Vela-Bueno, A., Kales, A., Soldatos, C.R., Dobladez-Blanco, B., Campos-Castello, J., Espino-Hurtado, P. and Olivan-Palacios, J. (1984) Sleep in the Prader–Willi syndrome. Clinical and polygraphic findings. *Arch. Neurol.*, **41**, 294–296.
9. Bruni, O., Verrillo, E., Novelli, L. and Ferri, R. (2010) Prader–Willi syndrome: sorting out the relationships between obesity, hypersomnia, and sleep apnea. *Curr. Opin. Pulm. Med.*, **16**, 568–573.
10. Clarke, D.J., Waters, J. and Corbett, J.A. (1989) Adults with Prader–Willi syndrome: abnormalities of sleep and behaviour. *J. R. Soc. Med.*, **82**, 21–24.
11. Tobias, E.S., Tolmie, J.L. and Stephenson, J.B. (2002) Cataplexy in the Prader–Willi syndrome. *Arch. Dis. Child.*, **87**, 170.
12. de Smith, A.J., Purmann, C., Walters, R.G., Ellis, R.J., Holder, S.E., Van Haelst, M.M., Brady, A.F., Fairbrother, U.L., Dattani, M., Keogh, J.M. *et al.* (2009) A deletion of the HBII-85 class of small nucleolar RNAs (snoRNAs) is associated with hyperphagia, obesity and hypogonadism. *Hum. Mol. Genet.*, **18**, 3257–3265.
13. Sahoo, T., del Gaudio, D., German, J.R., Shinawi, M., Peters, S.U., Person, R.E., Garnica, A., Cheung, S.W. and Beaudet, A.L. (2008) Prader–Willi phenotype caused by paternal deficiency for the HBII-85 C/D box small nucleolar RNA cluster. *Nat. Genet.*, **40**, 719–721.
14. Lassi, G., Priano, L., Maggi, S., Garcia-Garcia, C., Balzani, E., El-Assawy, N., Pagani, M., Tinarelli, F., Giardino, D., Mauro, A. *et al.* (2016) Deletion of the Snord116/SNORD116 alters sleep in mice and patients with Prader–Willi syndrome. *Sleep*, **39**, 637–644.
15. Powell, W.T. and LaSalle, J.M. (2015) Epigenetic mechanisms in diurnal cycles of metabolism and neurodevelopment. *Hum. Mol. Genet.*, **24**, R1–R9.
16. Steriade, M., McCormick, D.A. and Sejnowski, T.J. (1993) Thalamocortical oscillations in the sleeping and aroused brain. *Science*, **262**, 679–685.
17. Krol, A., Wimmer, R.D., Halassa, M.M. and Feng, G. (2018) Thalamic reticular dysfunction as a circuit endophenotype in neurodevelopmental disorders. *Neuron*, **98**, 282–295.
18. Gilboa, T. and Gross-Tsur, V. (2013) Epilepsy in Prader–Willi syndrome: experience of a national referral centre. *Dev. Med. Child Neurol.*, **55**, 857–861.
19. Hertz, G., Cataletto, M., Feinsilver, S.H. and Angulo, M. (1993) Sleep and breathing patterns in patients with Prader–Willi syndrome (PWS): effects of age and gender. *Sleep*, **16**, 366–371.
20. Zhang, Y., Zhao, H., Qiu, S., Tian, J., Wen, X., Miller, J.L., von Deneen, K.M., Zhou, Z., Gold, M.S. and Liu, Y. (2013) Altered functional brain networks in Prader–Willi syndrome. *NMR Biomed.*, **26**, 622–629.
21. Hinard, V., Mikhail, C., Pradervand, S., Curie, T., Houtkooper, R.H., Auwerx, J., Franken, P. and Tafti, M. (2012) Key electrophysiological, molecular, and metabolic signatures of sleep and wakefulness revealed in primary cortical cultures. *J. Neurosci.*, **32**, 12506–12517.
22. Trachsel, L., Tobler, I., Achermann, P. and Borbely, A.A. (1991) Sleep continuity and the REM-nonREM cycle in the rat under baseline conditions and after sleep deprivation. *Physiol. Behav.*, **49**, 575–580.
23. Toth, L.A. and Bhargava, P. (2013) Animal models of sleep disorders. *Comp. Med.*, **63**, 91–104.
24. Mitchell, H.A. and Weinshenker, D. (2010) Good night and good luck: norepinephrine in sleep pharmacology. *Biochem. Pharmacol.*, **79**, 801–809.
25. Mallick, B.N., Majumdar, S., Faisal, M., Yadav, V., Madan, V. and Pal, D. (2002) Role of norepinephrine in the regulation of rapid eye movement sleep. *J. Biosci.*, **27**, 539–551.
26. Colombi, I., Tinarelli, F., Pasquale, V., Tucci, V. and Chiappalone, M. (2016) A simplified in vitro experimental model encompasses the essential features of sleep. *Front. Neurosci.*, **10**, 315.
27. Eytan, D. and Marom, S. (2006) Dynamics and effective topology underlying synchronization in networks of cortical neurons. *J. Neurosci.*, **26**, 8465–8476.
28. Chiappalone, M., Vato, A., Berdondini, L., Koudelka-Hep, M. and Martinoia, S. (2007) Network dynamics and synchronous activity in cultured cortical neurons. *Int. J. Neural Syst.*, **17**, 87–103.
29. van Pelt, J., Wolters, P.S., Corner, M.A., Rutten, W.L. and Ramakers, G.J. (2004) Long-term characterization of firing dynamics of spontaneous bursts in cultured neural networks. *IEEE Trans. Biomed. Eng.*, **51**, 2051–2062.
30. Borbely, A.A. and Achermann, P. (1999) Sleep homeostasis and models of sleep regulation. *J. Biol. Rhythm.*, **14**, 557–568.
31. Amici, R., Cerri, M., Ocampo-Garces, A., Baracchi, F., Dentico, D., Jones, C.A., Luppi, M., Perez, E., Parmeggiani, P.L. and Zamboni, G. (2008) Cold exposure and sleep in the rat: REM sleep homeostasis and body size. *Sleep*, **31**, 708–715.
32. Amici, R., Zamboni, G., Perez, E., Jones, C.A. and Parmeggiani, P.L. (1998) The influence of a heavy thermal load on REM sleep in the rat. *Brain Res.*, **781**, 252–258.
33. Amici, R., Zamboni, G., Perez, E., Jones, C.A., Toni, I.I., Culin, F. and Parmeggiani, P.L. (1994) Pattern of desynchronized sleep during deprivation and recovery induced in the rat by changes in ambient temperature. *J. Sleep Res.*, **3**, 250–256.
34. Ursin, R. (1970) Sleep stage relations within the sleep cycles of the cat. *Brain Res.*, **20**, 91–97.
35. Merica, H. and Gaillard, J.M. (1991) A study of the interrupted REM episode. *Physiol. Behav.*, **50**, 1153–1159.
36. Zamboni, G., Perez, E., Amici, R., Jones, C.A. and Parmeggiani, P.L. (1999) Control of REM sleep: an aspect of the regulation of physiological homeostasis. *Arch. Ital. Biol.*, **137**, 249–262.
37. Zamboni, G., Amici, R., Perez, E., Jones, C.A. and Parmeggiani, P.L. (2001) Pattern of REM sleep occurrence in continuous darkness following the exposure to low ambient temperature in the rat. *Behav. Brain Res.*, **122**, 25–32.
38. Jones, C.A., Perez, E., Amici, R., Luppi, M., Baracchi, F., Cerri, M., Dentico, D. and Zamboni, G. (2008) Lithium affects REM sleep occurrence, autonomic activity and brain second messengers in the rat. *Behav. Brain Res.*, **187**, 254–261.
39. Zamboni, G., Jones, C.A., Domeniconi, R., Amici, R., Perez, E., Luppi, M., Cerri, M. and Parmeggiani, P.L. (2004) Specific changes in cerebral second messenger accumulation underline REM sleep inhibition induced by the exposure to low ambient temperature. *Brain Res.*, **1022**, 62–70.
40. Ferrarelli, F. and Tononi, G. (2017) Reduced sleep spindle activity point to a TRN-MD thalamus-PFC circuit dysfunction in schizophrenia. *Schizophr. Res.*, **180**, 36–43.
41. Fuentealba, P. and Steriade, M. (2005) The reticular nucleus revisited: intrinsic and network properties of a thalamic pacemaker. *Prog. Neurobiol.*, **75**, 125–141.
42. Sitnikova, E., Hramov, A.E., Grubov, V. and Koronovsky, A.A. (2014) Age-dependent increase of absence seizures and intrinsic frequency dynamics of sleep spindles in rats. *Neurosci. J.*, **2014**, 370764.
43. Andrillon, T., Nir, Y., Staba, R.J., Ferrarelli, F., Cirelli, C., Tononi, G. and Fried, I. (2011) Sleep spindles in humans: insights

from intracranial EEG and unit recordings. *J. Neurosci.*, **31**, 17821–17834.
44. Gruber, R. and Wise, M.S. (2016) Sleep spindle characteristics in children with neurodevelopmental disorders and their relation to cognition. *Neural Plast.*, **2016**, 4724792.
45. Burnett, L.C., Hubner, G., LeDuc, C.A., Morabito, M.V., Carli, J.F.M. and Leibel, R.L. (2017) Loss of the imprinted, non-coding Snord116 gene cluster in the interval deleted in the Prader–Willi syndrome results in murine neuronal and endocrine pancreatic developmental phenotypes. *Hum. Mol. Genet.*, **26**, 4606–4616.
46. Adhikari, A., Copping, N.A., Onaga, B., Pride, M.C., Coulson, R.L., Yang, M., Yasui, D.H., LaSalle, J.M. and Silverman, J.L. (2019) Cognitive deficits in the Snord116 deletion mouse model for Prader–Willi syndrome. *Neurobiol. Learn. Mem.*, **165**, 106874.
47. Taillard, J., Sagaspe, P., Berthomier, C., Brandewinder, M., Amieva, H., Dartigues, J.F., Rainfray, M., Harston, S., Micoulaud-Franchi, J.A. and Philip, P. (2019) Non-REM sleep characteristics predict early cognitive impairment in an aging population. *Front. Neurol.*, **10**, 197.
48. Weselake, S.V., Foulds, J.L., Couch, R., Witmans, M.B., Rubin, D. and Haqq, A.M. (2014) Prader–Willi syndrome, excessive daytime sleepiness, and narcoleptic symptoms: a case report. *J. Med. Case Rep.*, **8**, 127.
49. Eschenko, O., Magri, C., Panzeri, S. and Sara, S.J. (2012) Noradrenergic neurons of the locus coeruleus are phase locked to cortical up-down states during sleep. *Cereb. Cortex*, **22**, 426–435.
50. Geyer, M.A., Segal, D.S. and Mandell, A.J. (1972) Effect of intraventricular infusion of dopamine and norepinephrine on motor activity. *Physiol. Behav.*, **8**, 653–658.
51. Saberi-Moghadam, S., Simi, A., Setareh, H., Mikhail, C. and Tafti, M. (2018) In vitro cortical network firing is homeostatically regulated: a model for sleep regulation. *Sci. Rep.*, **8**, 6297.
52. O'Malley, M.W. and Datta, S. (2013) REM sleep regulating mechanisms in the cholinergic cell compartment of the brainstem. *Ind. J. Sleep Med.*, **8**, 58–66.
53. Colonnese, M.T., Kaminska, A., Minlebaev, M., Milh, M., Bloem, B., Lescure, S., Moriette, G., Chiron, C., Ben-Ari, Y. and Khazipov, R. (2010) A conserved switch in sensory processing prepares developing neocortex for vision. *Neuron*, **67**, 480–498.
54. Bergles, D.E., Doze, V.A., Madison, D.V. and Smith, S.J. (1996) Excitatory actions of norepinephrine on multiple classes of hippocampal CA1 interneurons. *J. Neurosci.*, **16**, 572–585.
55. Coulson, R.L., Yasui, D.H., Dunaway, K.W., Laufer, B.I., Vogel Ciernia, A., Zhu, Y., Mordaunt, C.E., Totah, T.S. and LaSalle, J.M. (2018) Snord116-dependent diurnal rhythm of DNA methylation in mouse cortex. *Nat. Commun.*, **9**, 1616.
56. Kobayashi, Y., Ye, Z. and Hensch, T.K. (2015) Clock genes control cortical critical period timing. *Neuron*, **86**, 264–275.
57. Habtemariam, S. (2018) The brain-derived neurotrophic factor in neuronal plasticity and neuroregeneration: new pharmacological concepts for old and new drugs. *Neural Regen. Res.*, **13**, 983–984.
58. Tornqvist, E., Annas, A., Granath, B., Jalkesten, E., Cotgreave, I. and Oberg, M. (2014) Strategic focus on 3R principles reveals major reductions in the use of animals in pharmaceutical toxicity testing. *PLoS One*, **9**, e101638.
59. Skryabin, B.V., Gubar, L.V., Seeger, B., Pfeiffer, J., Handel, S., Robeck, T., Karpova, E., Rozhdestvensky, T.S. and Brosius, J. (2007) Deletion of the MBII-85 snoRNA gene cluster in mice results in postnatal growth retardation. *PLoS Genet.*, **3**, e235.
60. Koehl, M., Battle, S. and Meerlo, P. (2006) Sex differences in sleep: the response to sleep deprivation and restraint stress in mice. *Sleep*, **29**, 1224–1231.
61. Pace, M., Camilo, M.R., Seiler, A., Duss, S.B., Mathis, J., Manconi, M. and Bassetti, C.L. (2018) Rapid eye movements sleep as a predictor of functional outcome after stroke: a translational study. *Sleep*, **41**, zsy138.
62. Pace, M., Adamantidis, A., Facchin, L. and Bassetti, C. (2017) Role of REM sleep, melanin concentrating hormone and orexin/hypocretin systems in the sleep deprivation preischemia. *PLoS One*, **12**, e0168430.
63. Liu, L. and Duff, K. (2008) A technique for serial collection of cerebrospinal fluid from the cisterna magna in mouse. *J. Vis. Exp.*, **21**, pii: 960.
64. El Merhie, A., Ito, D., Colombi, I., Keshavan, S., Mishra, N., Miseikis, V., Diaspro, A., Coletti, C., Chiappalone, M. and Dante, S. (2018) Single layer graphene functionalized MEA for enhanced detection of neuronal network development. *Sensors Actuat. B Chem.*, **277**, 224–233.
65. Cirelli, C. and Tononi, G. (2000) Differential expression of plasticity-related genes in waking and sleep and their regulation by the noradrenergic system. *J. Neurosci.*, **20**, 9187–9194.
66. Cirelli, C. and Tononi, G. (2000) Gene expression in the brain across the sleep-waking cycle. *Brain Res.*, **885**, 303–321.
67. Cirelli, C., Faraguna, U. and Tononi, G. (2006) Changes in brain gene expression after long-term sleep deprivation. *J. Neurochem.*, **98**, 1632–1645.
68. Schmitt, K., Holsboer-Trachsler, E. and Eckert, A. (2016) BDNF in sleep, insomnia, and sleep deprivation. *Ann. Med.*, **48**, 42–51.
69. Chomczynski, P. and Mackey, K. (1995) Short technical reports. Modification of the TRI reagent procedure for isolation of RNA from polysaccharide- and proteoglycan-rich sources. *BioTechniques*, **19**, 942–945.
70. Balzani, E., Falappa, M., Balci, F. and Tucci, V. (2018) An approach to monitoring home-cage behavior in mice that facilitates data sharing. *Nat. Protoc.*, **13**, 1331–1347.